Asian Journal of Chemistry; Vol. 34, No. 3 (2022), 619-626

ASIAN JOURNAL OF CHEMISTRY

https://doi.org/10.14233/ajchem.2022.23532

Study of Isotherm and Kinetic Parameters for Efficient Adsorption of Methylene Blue Dye onto the Surface of Meldrum's Acid Modified SPIONs

KEERTI RANI, JAIVEER SINGH, ARTI JANGRA, PARVIN KUMAR, SURESH KUMAR and RAMESH KUMAR*

Department of Chemistry, Kurukshetra University, Kurukshetra-136119, India

*Corresponding author: E-mail: rameshkumarkuk@gmail.com; rameshchemkuk@kuk.ac.in

Received: 14 September 2021; *Accepted*: 29 November 2021; *Published online*: 14 February 2022; AJC-20694

In present study, Meldrum's acid modified magnetite nanoparticles (MA-Fe_3O_4) were synthesized for the removal of methylene blue by co-precipitation method. These coated nanoparticles were examined by TGA, FESEM, XRD, FTIR and UV-vis analysis. The FESEM results depicted that mean size of modified superparamagnetic iron oxide nanoparticles (SPIONs) was about 30 nm. Meldrum's acid modified magnetic nanoparticles were found extremely effective in methylene blue dye adsorption from aqueous solution. The data obtained from isotherm study showed that adsorption process was consistent with Freundlich Model. Moreover, kinetic studies revealed that the adsorption of the dye on surface of coated magnetic nanoparticles followed pseudo-second order kinetics. Additionally, a comparative study has been made for the methylene blue dye removal efficiency by Meldrum's acid modified magnetic nanoparticles with already reported adsorbents.

Keywords: Adsorption, Methylene blue, Isotherm, Kinetics, Meldrum's acid, SPIONs.

INTRODUCTION

Dye is one of the major components among the pollutants present in the discharges of printing, tanning, textile, paper and cosmetic industries [1]. The wastewater discharges from these industries are identified by bright colour and high toxicity to marine biomes because the dyes present in the water block the sunlight transmission and thus prevent the photosynthesis of aquatic plants [2,3]. Therefore, the intense colour of water is considered as one of the clear indicator of the water pollution [4].

Methylene blue or urelene blue also named as basic blue 9, which is a cationic dye used in several purposes like dyeing textiles, a staining agent to make certain body fluids and tissues easier to view during surgery [5]. In spite of its valuable usage, methylene blue is a cancer causing agent and has been categorized as a recalcitrant molecule because of its poor metabolization by microorganisms due to which it can persist for extended periods in the environment. Its exposure can cause vomiting, eye irritation and chronic toxicity mainly to the central nervous system [6,7]. Hence, it is extremely important to suggest highly efficient, cheap and environmentally safe processes to abate methylene blue from the wastewater.

Various treatment methods have been already reported for dye removal such as membrane method, adsorption method, biodegradation and chemical oxidation [8]. Out of these methods, adsorption method considered as economical and extremely efficient method to follow due to its low cost and easy to perform [9]. Numerous researchers have used various adsorbents such as lemon grass leaf activated carbon [10], lead sulphide nanoparticles [11], sand [12], EDTA-modified bentonite [13], polyaniline nanofiber base [14], sludge ash [15], acid functionalized biomass [16], silica coated soya waste [17] and periodate-modified nanocellulose [18] for the degradation of methylene blue dye. Nanostructured materials have large surface to volume ratio so their surface can be easily functionalized using different molecules. Furthermore, nanoparticles act as an excellent adsorbent for the removal of dye due to their unique structural, optical and magnetic properties. Due to low toxicity, biocompatibility and high magnetic saturation superparamagnetic Fe_3O_4 nanoparticles appeared as a suitable candidate for modern technological applications [19]. Without surface coating Fe_3O_4 nanoparticles may be easily agglomerated in the course of chemical reaction. This phenomenon hinders the efficacy of Fe_3O_4 nanoparticles for the future applications [20].

The present work focused on the synthesis and characterization of Meldrum's acid modified SPIONs for methylene blue dye removal from the aqueous solutions. Moreover, isotherm and kinetic studies were performed for the abatement of methylene blue dye from aqueous solution onto the surface of modified superparamagnetic iron oxide nanoparticles (SPIONs).

EXPERIMENTAL

Ferrous sulfate heptahydrate ($FeSO_4 \cdot 7H_2O$, 98%), ferric chloride hexahydrate ($FeCl_3 \cdot 6H_2O$, 97%), ammonium hydroxide solution (25%), methylene blue and Meldrum's acid were acquired from SRL (India). Analytical graded chemicals were used without extra purification throughout the experimental work.

The infrared spectra of bare and Meldrum's acid (MA) coated magnetic nanoparticles were recorded using the MB-3000 ABB FTIR spectrometer. Absorbance measurements were obtained using a T90 PG Instrument Limited UV-visible spectrophotometer (900-190 nm). Thermal analysis of nanoparticles was performed by Perkin-Elmer STA-6000 thermo gravimetric analyzer (heating rate 5-80 ºC/min and the temperature range 20-1000 ºC). The average size of nanoparticles was monitored using the Hitachi SU-8000 field emission scanning electron microscope (FESEM). An instrument employing radiation (λ = 1.540 Å) was used to record X-ray diffraction (XRD) patterns at room temperature. A digital mechanical stirrer (2000 rpm) was used to synthesize magnetic nanoparticles.

Synthesis of Fe_3O_4 and MA-Fe_3O_4 nanoparticles: For synthesis of bare and Meldrum's acid (MA) coated magnetite nanoparticles co-precipitation method was used. Initially, 50 mL solution of ferrous sulphate was mixed with 50 mL solution of ferric chloride in molar ratio (2:1). The resultant solution was warmed upto 85 ºC by vigorous stirring (about 0.5 h) under inert gas atmosphere followed by the addition of 20 mL of ammonia solution into the reaction mixture until pH of the solution reached approximately 10. The formation of Fe_3O_4 nanoparticles was confirmed by colour change from brown to black [21]. Then, 1.25 g Meldrum's acid dissolved in 50 mL of water was added rapidly to the above solution and stirred further for 1 h. The Meldrum's acid coated iron oxide nanoparticles (IONPs) were separated from the solution by applying external magnetic field and washed with deionized water. Further, these surface modified magnetic nanoparticles were dried in oven (**Scheme-I**) and used for XRD, FTIR, FESEM and TG analysis.

Determination of methylene blue concentration: For methylene blue (50 ppm), the maximum absorption peak was appeared at 663 nm in the visible range. The concentration of solution was changed in the range (10-50 ppm) and their absorbance was determined at 663 nm. Calibration curve was achieved by plotting the graph between absorbance and concentration of methylene blue at maximum wavelength. A straight line graph was obtained with high regression coefficient ($R^2 = 0.978$) as shown in Fig. 1.

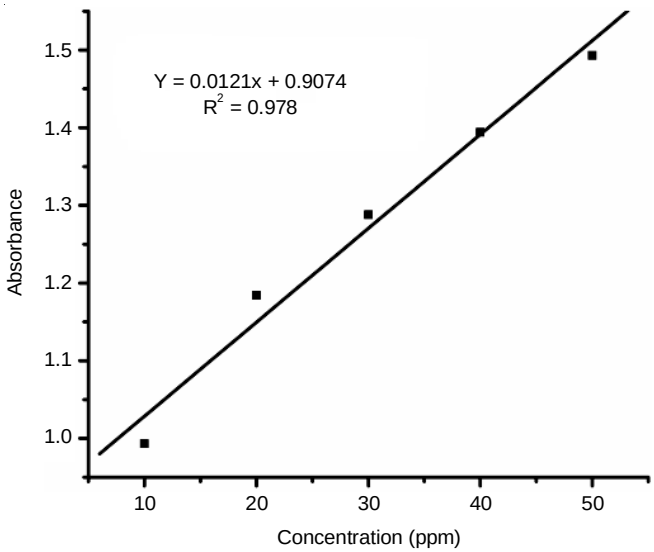

Fig. 1. Calibration curve to determine concentration of methylene blue

Adsorption experiments: The adsorption experiments were carried using batch adsorption process. The influences of experimental parameters such as adsorbent dose (5-30 mg), pH (3-7) and contact time (10-80 min) on the adsorptive removal of methylene blue were investigated in a batch mode. The equilibrium adsorption capacity (q_e) was calculated using eqn. 1 [22,23]:

$$q_e = \frac{(C_o - C_e)V}{m} \quad (1)$$

The percentage removal of dye was determined using eqn. 2 [24]:

$$R\ (\%) = \frac{C_o - C_e}{C_o} \times 100 \quad (2)$$

where, C_o = initial concentration of dye (ppm); C_e = dye residual concentration (ppm) at equilibrium; V = volume of methylene

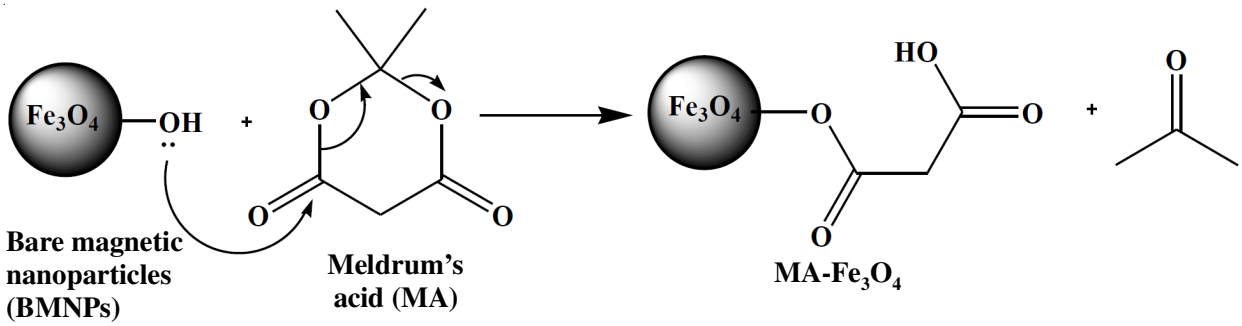

Scheme-I: Scheme for the synthesis of Meldrum's acid modified nanoparticles

blue dye solution (L) and m = adsorbent weight (g). The capacity of adsorption q_t (mg/g) at various contact time t (min) was calculated using eqn. 3 [25]:

$$q_t(mg/g) = \frac{(C_o - C_t)V}{m} \quad (3)$$

where, C_o = initial methylene blue concentration in ppm and C_t = methylene blue concentration at time 't' (min). To calculate the maximum capacity of adsorption, the amount of methylene blue dye adsorbed on the surface of MA-Fe_3O_4 was applied to the Langmuir, Freundlich and Tempkin isotherm models.

RESULTS AND DISCUSSION

Characterization of Fe_3O_4 and MA-Fe_3O_4 nanoparticles

IR studies: The IR spectra of bare Fe_3O_4 nanoparticles and modified Fe_3O_4 nanoparticles were obtained to determine the nature of associated functional groups and to confirm the coating on the surface of bare nanoparticles (Fig. 2). On comparing the IR spectra of bare and MA-Fe_3O_4, the various changes have been observed in the IR spectra of MA-Fe_3O_4. Firstly, a characteristic absorption band at 2954 cm^{-1} is considered as the stretching corresponds to the active methylene group. Secondly, a sharp band appears at 1748 cm^{-1} indicated the ester group formation during the esterification reaction. Lastly, the bands appearing at 1590 cm^{-1} and 1384 cm^{-1} correspond to the carboxylate group. Thus, it can be stated that the esterification reaction was successful between the pure Meldrum's acid and bare magnetic nanoparticles. Additionally, a common peak is observed in the IR spectra of both *i.e.* bare Fe_3O_4 and MA-Fe_3O_4 nanoparticles which may be due to Fe-O stretching.

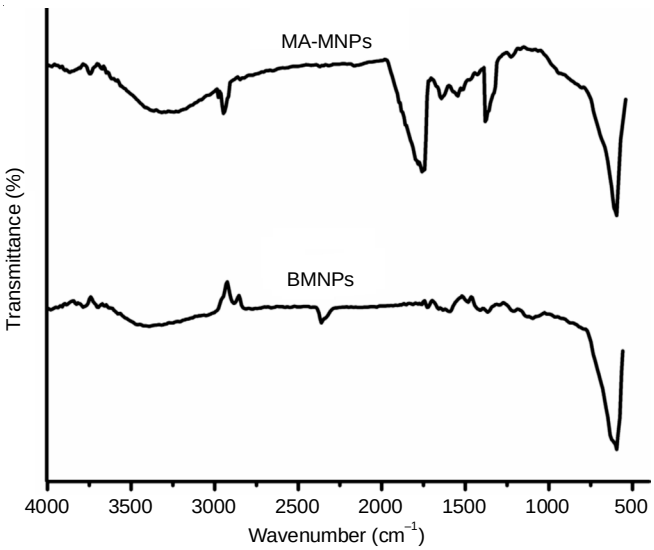

Fig. 2. FTIR spectra of bare magnetic nanoparticles (BMNPs) and Meldrum's acid coated magnetic nanoparticles (MA-MNPs)

X-ray diffraction (XRD) studies: The crystalline nature and crystal structure of the synthesized nanoparticles were studied by X-ray diffractometer in the range of 2θ between 20º and 80º. The XRD patterns of Fe_3O_4 and MA-Fe_3O_4 are displayed in Fig. 3. The pattern obtained exhibits sharp peaks for all the synthesized magnetic nanoparticles. The diameters

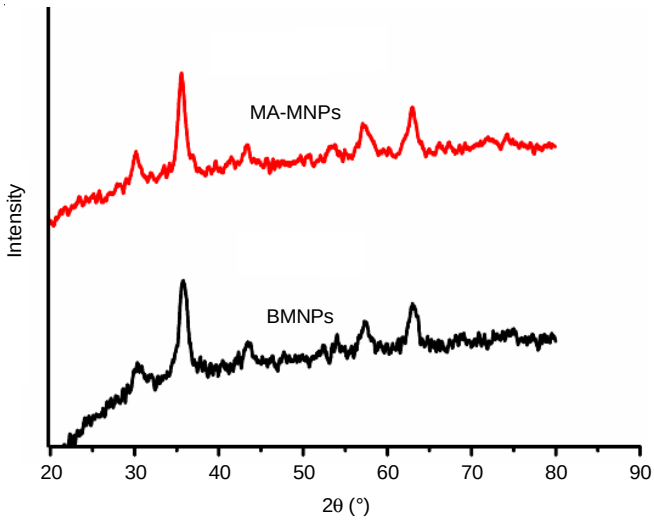

Fig. 3. XRD pattern of bare magnetic nanoparticles (BMNPs) and Meldrum's acid coated magnetic nanoparticles (MA-MNPs)

of the nanoparticles were calculated by using the Scherrer equation (eqn. 4) [26]:

$$d = \frac{0.9\lambda}{\beta\cos\theta} \quad (4)$$

where, λ is the source wavelength , β is the line broadening at half-height of the maximum intensity of the peak and θ is the Bragg angle. By putting the full width at half maximum (FWHM) of the most intense peak into the Scherrer's equation, the average sizes of particles were calculated as 11.69 nm and 13.60 nm for bare Fe_3O_4 and MA coated Fe_3O_4 nanoparticles, respectively. Interestingly, the size of bare and coated magnetic nanoparticles calculated from Scherrer's equation was found in close agreement with the results obtained from FESEM study.

FESEM studies: Field emission scanning electron (FESEM) microscopy study of bare and Meldrum's acid coated magnetite nanoparticles reveals the coating of Meldrum's acid on the surface of bare nanoparticles as the average particle size of prepared Fe_3O_4 and Meldrum's acid coated Fe_3O_4 magnetic nanoparticles was found to be 20 and 30 nm, respectively (Fig. 4). An increase in the size of Fe_3O_4 MNPs after coating suggested the successful coating of Meldrum's acid on the surface of bare Fe_3O_4 magnetic nanoparticles.

Thermogravimetric analysis (TGA): TGA curves of bare and MA coated Fe_3O_4 nanoparticles were obtained to investigate their thermal behaviour (Fig. 5). The initial weight loss for both *i.e.* uncoated and coated iron oxide nanoparticles (IONPs) within the region 10-150 ºC may be linked with the vaporization of adsorbed water. Above 200 ºC, the weight loss for Meldrum's acid coated iron oxide nanoparticles was observed which is due to the decomposition of Meldrum's acid coating from the surface of iron oxide nanoparticles. Although, in case of pure Meldrum's acid the corresponding degradation was observed at low temperature inferring that thermal stability was enhanced after coating. However, no significant weight loss was observed beyond 400 ºC which is probably related to iron oxide nanoparticles. From TG curves of bare and Meldrum's acid coated iron oxide nanoparticles, it was clear that the net

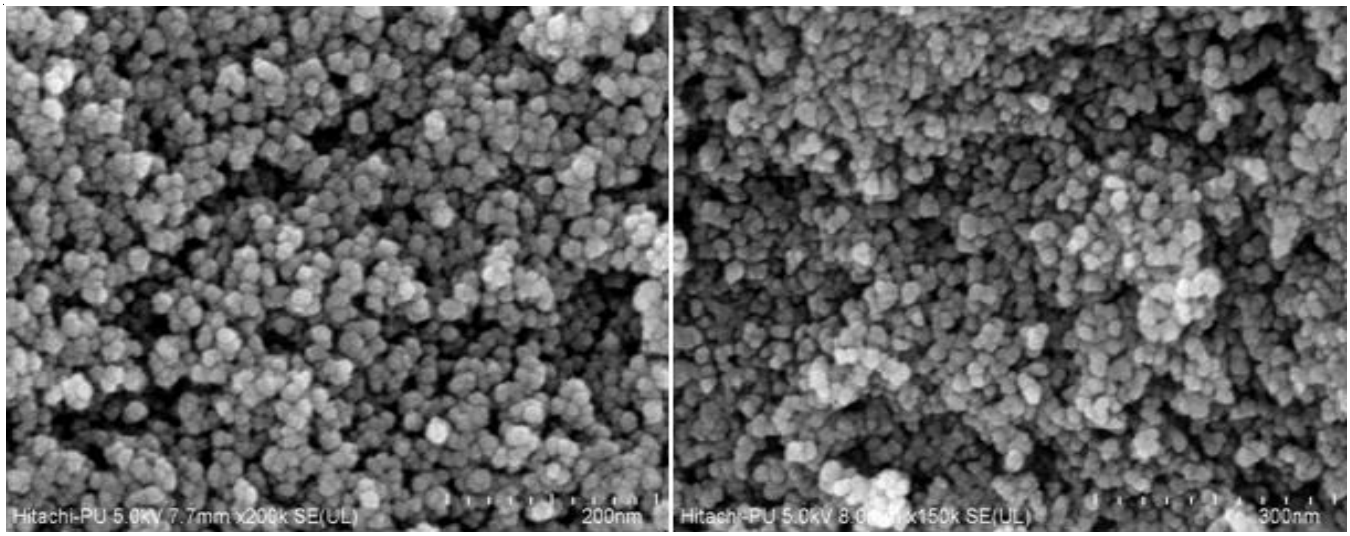

Fig. 4. FESEM image of bare magnetic nanoparticles (BMNPs) [1 division = 20 nm] and Meldrum's acid coated magnetic nanoparticles (MA-MNPs) [1 division = 30 nm]

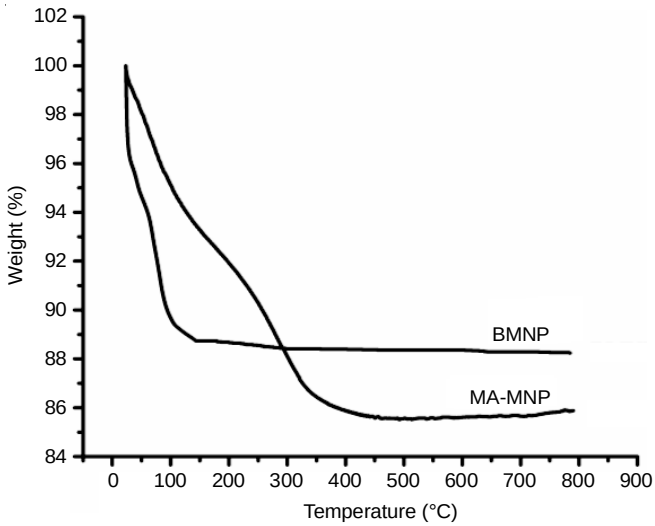

Fig. 5. TGA curves of bare magnetic nanoparticles (BMNPs) and Meldrum's acid coated magnetic nanoparticles (MA-MNPs)

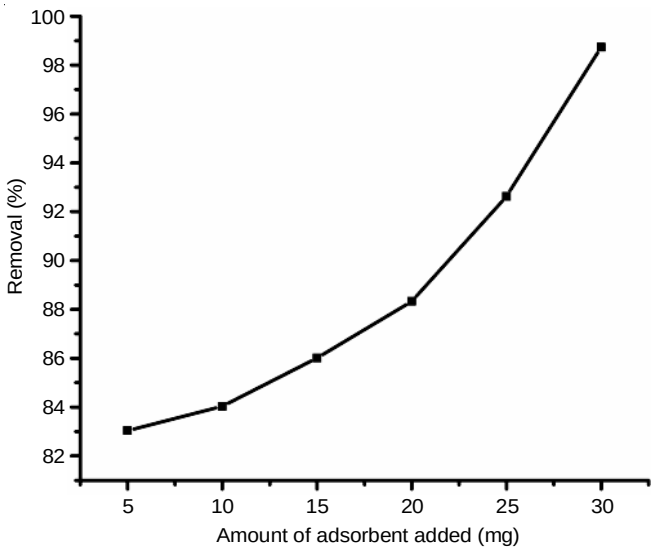

Fig. 6. Effect of adsorbent dosage on the removal efficiency

weight loss for Fe_3O_4 and MA coated Fe_3O_4 nanoparticles was 11.67 % and 14.12 %, respectively.

Adsorption studies of Meldrum's acid (MA) coated Fe_3O_4 with variation in different parameters: The influence of different adsorption parameters *i.e.* the effect of the dosage, contact time, effect of pH and effect of dye initial concentration on the removal of methylene blue dye was investigated by synthesized MA-Fe_3O_4.

Effect of MA coated Fe_3O_4 MNPs dosage: The effect of the adsorbent dosage on the adsorption of methylene blue dye was examined using different amounts of adsorbent (5-30 mg) as shown in Fig. 6. Adsorption percentage was increased with increase in the amount of adsorbent due to the availability of many adsorption sites. When the amount of adsorbent was increased from 5 to 30 mg, methylene blue dye removal percentage was increased up to 98.74%. The removal efficiency MA-Fe_3O_4 nanoparticles is higher than Fe_3O_4 nanoparticles because the coating material provides extra binding sites through the electrostatic attraction between the functional group of Meldrum's acid and the dye molecule.

Effect of contact time: The influence of contact time on the removal efficiency of methylene blue dye was studied using the optimal conditions *i.e.* adsorbent dosage (30 mg) and concentration of methylene blue (50 ppm) at different times (10-80 min) as presented in Fig. 7. The maximum adsorption of the methylene blue dye appears at 60 min which is rapid equilibrium rate.

Effect of pH: To investigate the effect of pH on methylene blue adsorption, 30 mg of adsorbent was added to methylene blue dye solution (50 ppm) at various pH values (pH = 3-7) as shown in Fig. 8. The acidic and basic solutions were attained by adding dilute solution of HCl and NaOH, respectively. Removal percentage (%R) was increased by raising the pH of the solution because the strong electrostatic interaction between molecule of methylene blue dye (a cationic dye) and the carboxylate group (with anionic charge) of MA coated Fe_3O_4 nanoparticles.

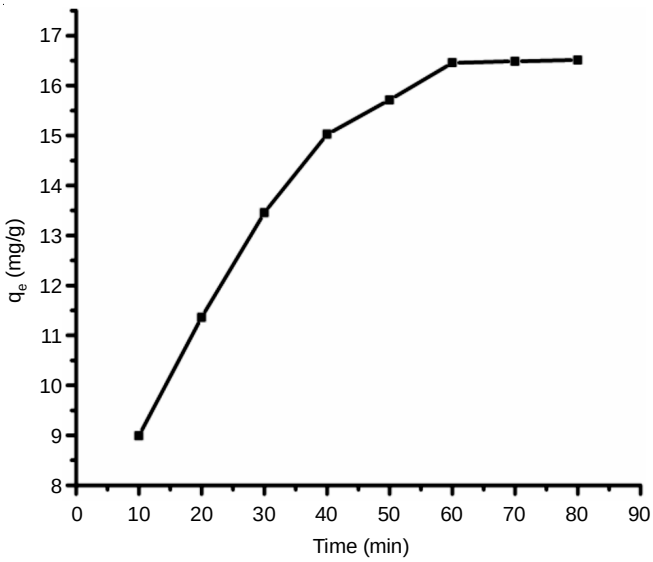

Fig. 7. Effect of contact time

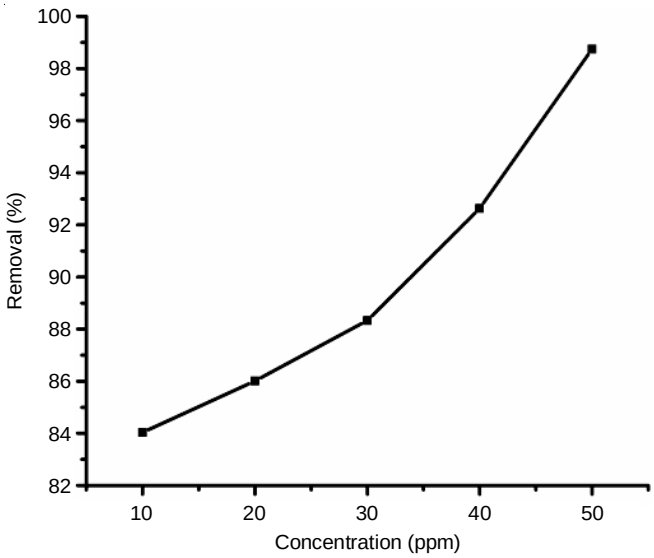

Fig. 9. Effect of initial concentration

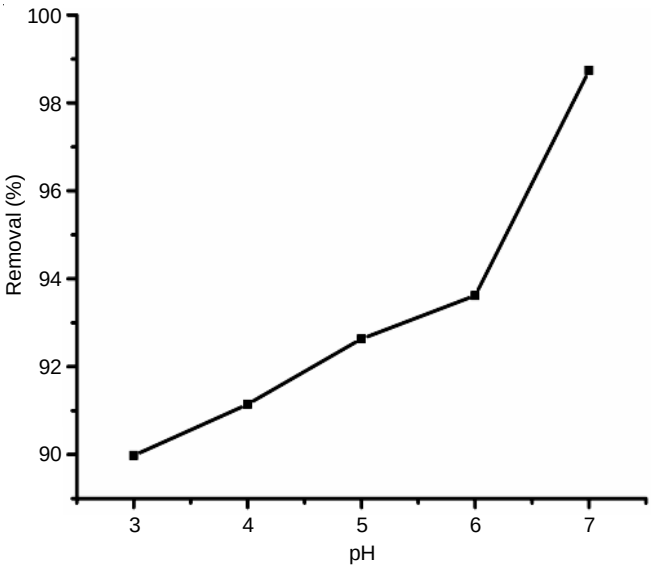

Fig. 8. Effect of pH on removal efficiency

Effect of initial concentration: The influence of initial concentration of methylene blue (10-50 ppm) on the adsorption capacity of Meldrum's acid coated magnetic nanoparticles was investigated under the specific conditions *i.e.* contact time (60 min) and amount of adsorbent added (5 mg) at room temperature. The removal efficiency was dependent upon the initial concentration of methylene blue as an increase in the removal efficiency was noticed with the decrease in the dye initial concentration as shown in Fig. 9.

Adsorption kinetic study: Adsorption kinetics is a significant parameter for designing adsorption systems [27]. The kinetic mechanism of adsorption was also investigated using the pseudo-first order kinetic model and the pseudo-second order kinetic model. The pseudo-first order kinetic model equation can be written as follows [28]:

$$\log(q_e - q_t) = \log q_e - \frac{k_1 t}{2.303} \quad (5)$$

where, q_e is the adsorption capacity at equilibrium time in mg/g, q_t (mg/g) is the adsorption capacity at time t (min) and k_1 is the rate constant of pseudo-first order kinetic model [29].

The pseudo-second order kinetic equation is calculated by using eqn. 6 [30]:

$$\frac{1}{q_t} = \frac{1}{k_2 q_e^2} + \frac{t}{q_e} \quad (6)$$

where k_2 is the rate constant of pseudo-second order. The order of kinetic model can be determined by plotting the graphs of log ($q_e - q_t$) *versus* t for pseudo-first order and t/q_t *versus* t for pseudo-second order as presented in Fig. 10. Moreover, the correlation factor ($R^2 = 0.994$) calculated from pseudo-second order kinetic model was higher than that of pseudo-first order kinetic model (Table-1). This suggested that the experimental data were in accordance with the pseudo-second order model.

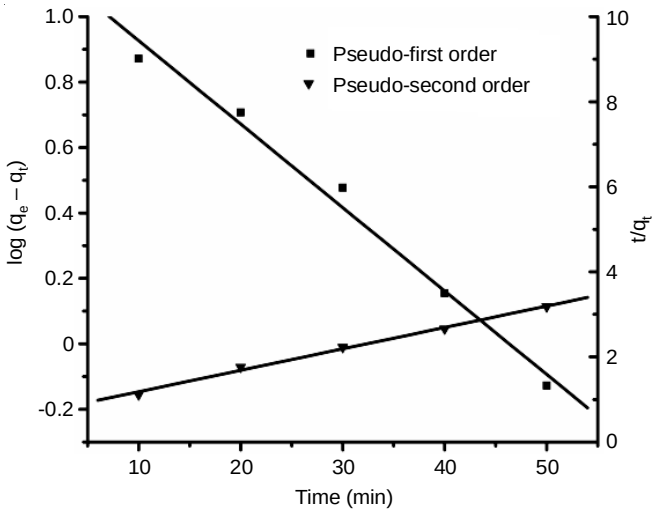

Fig. 10. Pseudo-first order and pseudo-second order kinetic plots

Adsorption isotherms: The isotherm study describes the interactions between adsorbate and adsorbent. Langmuir, Freundlich and Tempkin isotherms were discussed in this study

TABLE-1
CALCULATED KINETIC PARAMETERS FROM THE KINETIC GRAPHS FOR THE ADSORPTION OF METHYLENE BLUE DYE ONTO THE SURFACE OF MELDRUM'S ACID COATED IRON OXIDE NANOPARTICLES

Pseudo-first order kinetic model			Pseudo-second order kinetic model		
R^2	k_1 (min^{-1})	q_e (mg/g)	R^2	k_2 (g mg^{-1} min^{-1})	q_e (mg/g)
0.986	0.058	15.240	0.994	0.00375	19.833

[31]. The Langmuir theory describes a homogenous adsorption which reveals that when a molecule of dye occupies an adsorption site then no additional adsorption can take place at that site. The Langmuir model equation can be given as [32]:

$$\frac{C_e}{q_e} = \frac{1}{q_m K_L} + \frac{C_e}{q_m} \quad (7)$$

where C_e is the equilibrium concentration, q_m is the maximum adsorption capacity, q_e is adsorption capacity at equilibrium and K_L is the Langmuir constant. Langmuir isotherm graph was plotted between C_e/q_e and C_e as presented in the Fig. 11. Langmuir isotherm parameters *i.e.* q_m and K_L can be calculated with the help of slope and intercept as mentioned in Table-2. From the graph, the correlation coefficient (R^2) for Langmuir isotherm was found to be 0.942.

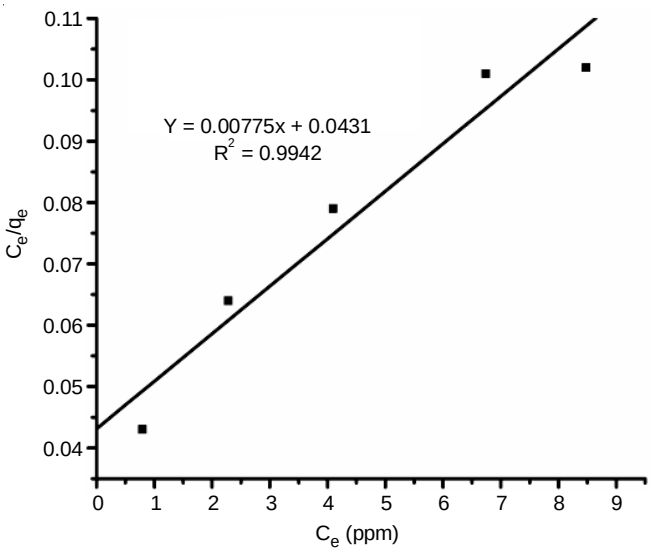

Fig. 11. Langmuir isotherm

Freundlich theory assumes a heterogeneous adsorption, which implies that various sites with different adsorption energies are involved. It is the relationship between the concentration and the amount adsorbed at equilibrium. The Freundlich isotherm equation is written as follow [33]:

$$\log q_e = \log K_F + \frac{1}{n}\log C_e \quad (8)$$

where K_F is the Freundlich constant and 1/n is a constant which represents the adsorption intensity. Freundlich isotherm graph was plotted between log q_e and log C_e as shown in the Fig. 12. The Freundlich parameters *i.e.* K_L and n were calculated with the help of slope and intercept as presented in Table-2. From the graph, the correlation coefficient (R^2) for Freundlich isotherm was found to be 0.997.

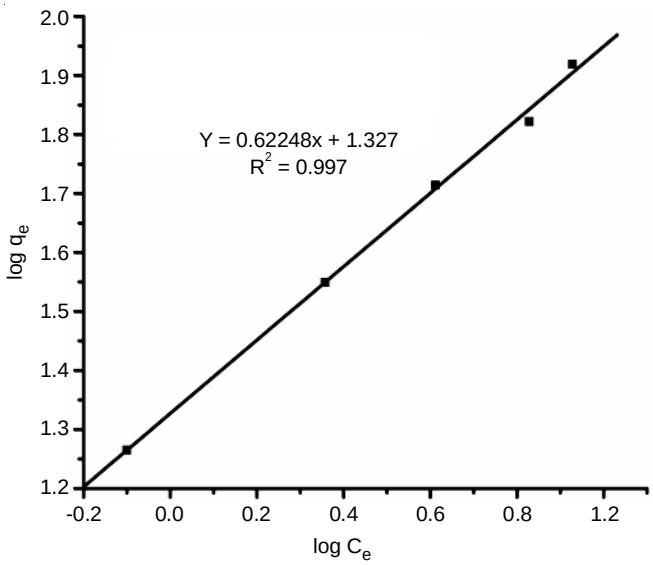

Fig. 12. Freundlich isotherm

Tempkin isotherm supposes that the adsorption heat of all molecules reduces in a linear manner in the layer due to the interactions between adsorbent and adsorbate. In addition, the adsorption is identified by the homogenous distribution of binding energies. Tempkin isotherm equation can be given in the following form [34]:

$$q_e = \frac{RT}{b}\ln K_T + \frac{RT}{b}\ln C_e \quad (9)$$

where K_T is the Tempkin isotherm constant and RT/b is equals to B that is a constant which represents the heat of sorption. Tempkin isotherm graph was plotted between q_e and ln C_e as shown in Fig. 13. The Tempkin isotherm parameters *i.e.* K_T and b were calculated with the help of slope and intercept as presented in Table-2. From the graph, the correlation coefficient for Tempkin isotherm was found to be 0.776. From the above

TABLE-2
ISOTHERM PARAMETERS CALCULATED FROM THE ISOTHERM GRAPHS FOR THE ADSORPTION OF METHYLENE BLUE DYE ONTO THE SURFACE OF MODIFIED SPIONs

Langmuir model			Freundlich model			Tempkin model		
R^2	q_m (mg/g)	K_L	R^2	K_F	n	R^2	K_T	B = RT/b
0.942	129.032	0.179	0.997	21.232	1.606	0.776	28.216	12.365

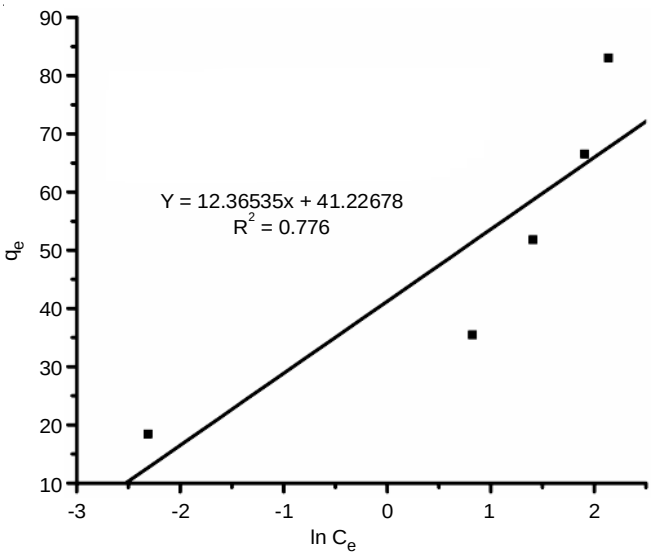

Fig. 13. Tempkin isotherm

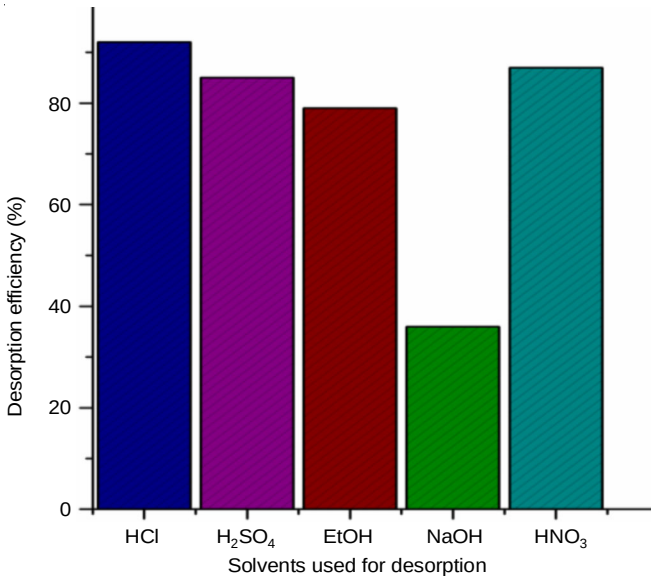

Fig. 14. Desorption study with various solvents

results, it was concluded that the adsorption isotherm best fitted with Freundlich model with high correlation coefficients (R^2 = 0.997). Also, the high value of R^2 for Freundlich model suggested the heterogeneous adsorption through a monolayer over the adsorbent surface. Moreover, adsorption of methylene blue dye from aqueous solution on the surface of MA-Fe_3O_4 nanoparticles was physisorption in nature.

Desorption study: The reusability is a crucial factor to judge the applications [35]. Meldrum's acid modified nanoparticles desorption data were obtained by performing the experiments in batch mode. Numerous solvents such as 0.1 M HCl, 0.1 M NaOH, 0.1 M HNO_3, 0.1 M H_2SO_4 and ethanol were used for the desorption of methylene blue dye from the surface of the modified nanoparticles. From the results, one can conclude that HCl shows better elution than the rest of the solvents and the percentage of desorption of methylene blue dye by hydrochloric acid solvent was about 92% (Fig. 14). These results are in good agreements with the effect of pH because the methylene blue dye shows the highest removal efficiency at basic pH. As the pH of the system decreases, the availability of positively charged sites on adsorbent was increased and an adsorbent having positively charged sites favours desorption of cationic dye by virtue of the electrostatic repulsion between the cationic dye and the positively charged adsorbent. Therefore, Meldrum's acid modified nanoparticles exhibit magnificent adsorption capacity and regeneration. Also, their further applications can be expanded for wastewater treatment from various industries.

Comparative study of removal of methylene blue dye by Meldrum's acid modified SPIONs with other reported adsorbents: The maximum percentage removal used in this study along with other reported adsorbents for the removal of methylene blue dye were summarized in Table-3. It can be observed that other reported adsorbents were less effective for removal of methylene blue dye in comparison of Meldrum's acid modified nanoparticles. Hence MA-Fe_3O_4 nanoparticles have been found as a potential adsorbent tool for the removal of methylene blue dye from aqueous solution.

TABLE-3
COMPARING THE PERCENTAGE REMOVAL OF METHYLENE BLUE DYE BY THE ADSORBENT USED IN THIS STUDY WITH OTHER REPORTED ADSORBENTS

Adsorbent	Removal (%)	Ref.
Lemon grass leaf activated carbon	64.36	[10]
Lead sulphide nanoparticles	75.90	[11]
Sand	92.00	[12]
EDTA-modified bentonite	40.00	[13]
Polyaniline nanofiber base	91.00	[14]
Sludge ash	80.00	[15]
Acid-factionalised biomass	83.00	[16]
Silica coated soya waste	97.10	[17]
Periodate-modified nanocellulose	78.10	[18]
Meldrum's acid modified SPIONs	98.74	This study

Conclusion

Meldrum's acid modified Fe_3O_4 (MA-Fe_3O_4) and bare Fe_3O_4 nanoparticles were synthesized by the chemical co-precipitation process and used for adsorptive removal of cationic methylene blue dye. Various physico-chemical characterizations suggested the effective coating on the surface of Fe_3O_4 nanoparticles. Batch adsorption studies revealed that adsorption of methylene blue dye varies with change in different parameters such as adsorbent dose, contact time, pH and initial concentration of dye. Adsorption kinetics results suggested that the methylene blue adsorption over the surface of MA-Fe_3O_4 nanoparticles obeyed pseudo-second order kinetics. Further, the adsorption isotherm data best fitted with the Freundlich isotherm model. The desorption study was also performed with different solvents. Hence, from the present study it can be concluded that MA-Fe_3O_4 nanoparticles can be used as a potential adsorbent tool for the removal of methylene blue dye from aqueous solution.

ACKNOWLEDGEMENTS

Co-authors, Keerti Rani, Jaiveer Singh and Arti Jangra are highly thankful to Kurukshetra University, Kurukshetra for providing research facilities. The authors acknowledge

UGC, New Delhi, India, for providing financial support in the form of a Senior Research Fellowship.

CONFLICT OF INTEREST

The authors declare that there is no conflict of interests regarding the publication of this article.

REFERENCES

1. E. Routoula and Siddharth V. Patwardhan, *Environ. Sci. Technol.*, **54**, 647 (2020); https://doi.org/10.1021/acs.est.9b03737
2. M. Hassanimarand, M. Anbia and S. Salehi, *ChemistrySelect*, **5**, 6141 (2020); https://doi.org/10.1002/slct.202000624
3. M. Berradi, R. Hsissou, M. Khudhair, M. Assouag, O. Cherkaoui, A. El-Bachiri and A. El-Harfia, *Heliyon*, **5**, e02711 (2019); https://doi.org/10.1016/j.heliyon.2019.e02711
4. F.P. Almeida, M.B.S. Botelho, C. Doerenkamp, E. Kessler, C.R. Ferrari, H. Eckert and A.S.S. de Camargo, *J. Solid State Chem.*, **253**, 406 (2017); https://doi.org/10.1016/j.jssc.2017.06.018
5. O.S. Bayomie, H. Kandeel, T. Shoeib, H. Yang, N. Youssef and M.M.H. El-Sayed, *Sci. Rep.*, **10**, 7824 (2020); https://doi.org/10.1038/s41598-020-64727-5
6. A.H. Jawad, S. Sabar, M.A.M. Ishak, L.D. Wilson, S.S. Ahmad Norrahma, M.K. Talari and A.M. Farhan, *Chem. Eng. Commun.*, **204**, 1143 (2017); https://doi.org/10.1080/00986445.2017.1347565
7. A.H. Jawad and A.S. Abdulhameed, *Surf. Interfaces*, **18**, 100422 (2020); https://doi.org/10.1016/j.surfin.2019.100422
8. R. Saxena, M. Saxena and A. Lochab, *ChemistrySelect*, **5**, 335 (2020); https://doi.org/10.1002/slct.201903542
9. X. Qi, Q. Zeng, X. Tong, T. Su, L. Xie, K. Yuan, J. Xu and J. Shen, *J. Hazard. Mater.*, **402**, 123359 (2021); https://doi.org/10.1016/j.jhazmat.2020.123359
10. M.A. Ahmad, N.B. Ahmed, K.A. Adegoke and O.S. Bello, *Chem. Data Coll.*, **31**, 100578 (2021); https://doi.org/10.1016/j.cdc.2020.100578
11. P.A. Ajibade, T.B. Mbuyazi and A.E. Oluwalana, *J. Inorg. Organomet. Polym. Mater.*, **31**, 2197 (2021); https://doi.org/10.1007/s10904-021-01957-8
12. S.B. Bukallah, M.A. Rauf and S.S. AlAli, *Dyes Pigments*, **74**, 85 (2007); https://doi.org/10.1016/j.dyepig.2006.01.016
13. M.L.F.A. De Castro, M.L.B. Abad, D.A.G. Sumalinog, R.R.M. Abarca, P. Paoprasert and M.D.G. de Luna, *Sustain. Environ. Res.*, **28**, 197 (2018); https://doi.org/10.1016/j.serj.2018.04.001
14. M. Duhan and R. Kaur, *J. Compos. Sci.*, **5**, 7 (2020); https://doi.org/10.3390/jcs5010007
15. C.H. Weng and Y.F. Pan, *Colloids Surf. A Physicochem. Eng. Asp.*, **274**, 154 (2006); https://doi.org/10.1016/j.colsurfa.2005.08.044
16. A.H. Jawad, A.S. Abdulhameed and M.S. Mastuli, *J. Taibah Univ. Sci.*, **14**, 305 (2020); https://doi.org/10.1080/16583655.2020.1736767
17. A. Batool and S. Valiyaveettil, *J. Environ. Chem. Eng.*, **9**, 104902 (2021); https://doi.org/10.1016/j.jece.2020.104902
18. H. Tsade Kara, S.T. Anshebo, F.K. Sabir and G.A. Workineh, *Int. J. Chem. Eng.*, **2021**, 9965452 (2021); https://doi.org/10.1155/2021/9965452
19. P. Li, W. Xiao, P. Chevallier, D. Biswas, X. Ottenwaelder, M.A. Fortin and J.K. Oh, *ChemistrySelect*, **1**, 4087 (2016); https://doi.org/10.1002/slct.201601035
20. G. Zhao, J.J. Feng, Q.L. Zhang, S.P. Li and H.Y. Chen, *Chem. Mater.*, **17**, 3154 (2005); https://doi.org/10.1021/cm048078s
21. J. Singh, A. Jangra, J. Kumar, K. Rani and R. Kumar, *Rasayan J. Chem.*, **13**, 105 (2020); https://doi.org/10.31788/RJC.2020.1315382
22. A. Günay, E. Arslankaya and I. Tosun, *J. Hazard. Mater.*, **146**, 362 (2007); https://doi.org/10.1016/j.jhazmat.2006.12.034
23. H.A. Al-Aoh, M.J. Maah, R. Yahya and M.R. Bin Abas, *Asian J. Chem.*, **25**, 9582 (2013); https://doi.org/10.14233/ajchem.2013.15082A
24. T. Saeed, A. Naeem, T. Mahmood, Z. Ahmad, M. Farooq, I.U. Farida, I.U. Din and I.W. Khan, *Int. J. Environ. Sci. Technol.*, **18**, 659 (2021); https://doi.org/10.1007/s13762-020-02844-4
25. K.K. Singh, K.K. Senapati and K.C. Sarma, *J. Environ. Chem. Eng.*, **5**, 2214 (2017); https://doi.org/10.1016/j.jece.2017.04.022
26. T.A. Saleh and V.K. Gupta, *Sep. Purif. Technol.*, **89**, 245 (2012); https://doi.org/10.1016/j.seppur.2012.01.039
27. S. Kamal Ghadiri, H. Alidadi, N.T. Nezhad, A. Javid, A. Roudbari, S.S. Talebi, A.A. Mohammadi, M. Shams and S. Rezania, *PLoS One*, **15**, e0231045 (2020). https://doi.org/10.1371/journal.pone.0231045
28. K.D. Kowanga, E. Gatebe, G.O. Mauti and E.M. Mauti, *J. Phytopharm.*, **5**, 71 (2016); https://doi.org/10.31254/phyto.2016.5206
29. W. Li, J. Liu, Y. Qiu, C. Li, W. Wang and Y. Yang, *J. Dispers. Sci. Technol.*, **40**, 1338 (2019); https://doi.org/10.1080/01932691.2018.1511436
30. D. Robati, *J. Nanostruct. Chem.*, **3**, 55 (2013); https://doi.org/10.1186/2193-8865-3-55
31. S. Singh and R. Jaiswal, *Res. J. Chem. Sci.*, **7**, 24 (2017).
32. N. Ayawei, A.N. Ebelegi and D. Wankasi, *J. Chem.*, **2017**, 3039817 (2017); https://doi.org/10.1155/2017/3039817
33. S. Sun, C. Zhai and J. Liu, *ChemistrySelect*, **5**, 1157 (2020); https://doi.org/10.1002/slct.201903600
34. E. Khaledyan, K. Alizadeh and Y. Mansourpanah, *Iran. J. Sci. Technol. Trans. A Sci.*, **43**, 801 (2019); https://doi.org/10.1007/s40995-018-0571-3
35. F. Buendia-Kandia, N. Brosse, D. Petitjean, G. Mauviel, E. Rondags, E. Guedon and A. Dufour, *Biomass Convers. Biorefin.*, **10**, 1 (2020); https://doi.org/10.1007/s13399-019-00395-4